REVISTA MATÉRIA V.29 N.2
ISSN 1517-7076 articles e20240040, 2024

# Interlayer bonding properties of 3D printed mortar with three types of inorganic coatings

Weihong Li[1], Xuhao Chen[1], Yongjie Deng[1], Detian Wan[2], Yaoyu Wang[1,3]

[1]Dalian University, Key Laboratory for Prediction & Control on Complicated Structure System of the Education. Xuefu Road, 10, 116622, Dalian, China.

[2]China Building Materials Academy, State Key Laboratory of Green Building Materials. Guanzhuang Dongli, 1, 100024, Chaoyang District, Beijing, China.

[3]Dalian University of Technology, School of Civil Engineering. Linggong Road, 2, 116024, Ganjingzi District, Dalian, China.

e-mail: liweihong714@163.com, chenxuhao997@163.com, Dengyongjie825@163.com, dtwan@ctc.ac.cn, wangyaoyuhappy@163.com

## ABSTRACT

This study explores the use of commonly utilized materials (sulphoaluminate cement, fly ash, expanding agent) in the creation of three inorganic coatings (C-coating, F-coating, E-coating) to improve the interlayer bonding properties of 3D printed mortar. The mechanical properties of mortar with/without coating were characterized by compressive test and flexural test. The bonding properties of the coatings were assessed through splitting tests and micron indentation tests. X-ray diffraction (XRD) and scanning electron microscopy (SEM) were employed to analyze the characteristics of hydration products and pore structure. The findings demonstrate that both F-coating and E-coating significantly enhance the mechanical properties of 3D printed mortar. Specifically, F-coating led to a 42% increase in flexural strength and a 71% increase in bond strength. The XRD and SEM analyses revealed that the fly ash contained in F-coating has a pozzolanic effect by reducing the content of $Ca(OH)_2$ (CH), promoting the formation of calcium silicate hydrate (C-S-H) gel, and enhancing microscopic morphology. The expansion agent contained in the E-coating could significantly increase the content of AFt, and the needle-like AFt plays a good bonding performance between the interfaces. In this manuscript, two kinds of cheap and easy-to-obtain interlayer coatings for 3D printing mortar are found.

**Keywords:** 3D printed mortar; weakness zone; inorganic coating; interlayer bonding properties.

## 1. INTRODUCTION

The 3D printing technology of concrete is based on the mathematical model, and the concrete is made into a three-dimensional entity in a layer-by-layer stacking way through the printing equipment [1-4]. This technology integrates various advanced technologies such as computer science, numerical control, material science, and information engineering [5–7]. Compared with traditional concrete technology, 3D printing technology could reduce waste, labor costs and production time [8–11].

Based on the existing technology, it is difficult for researchers to build an effective reinforcement system in 3D printed concrete buildings [12, 13]. As a result, these buildings often rely solely on the physical and mechanical properties of concrete to ensure structural safety [14]. However, the weak layer of 3D printed concrete has significantly lower mechanical properties compared to traditional concrete [15, 16]. This weakness directly impacts the overall mechanical properties of 3D printed concrete structures, compromising their safety, service life, and limiting the practical application and development of concrete 3D printing technology.

The current research results show that the mechanism of the weak zone between the printed concrete layers is closely related to the printing process (printing time, printing height, printing thickness, printing speed, etc.), geometric factors (area of the extrusion nozzle, geometry of the extrusion nozzle, etc.), physical factors (air content in concrete, porosity of concrete, etc.) and material factors (setting time, fluidity, etc.) [17, 18]. In order to improve the interlayer bonding of printed concrete, researchers around the world have carried out a lot of research work. PAN *et al*. [19] added nano clay to the 3D printed cement mortar to reduce the water loss in the weak zone, and improved the bonding strength between the layers by reducing the width of the weak zone.

Corresponding Author: Yaoyu Wang Received on 06/02/2024 Accepted on 16/05/2024

DOI: https://doi.org/10.1590/1517-7076-RMAT-2024-0040

LI *et al*. [20] added 1.5% viscosity modifier into the 3D printed mortar for increasing the water retention of the materials, reducing the bleeding phenomenon of the materials, promoting the hydration reaction and improving the interlayer bonding properties, so that the flexural strength and fracture energy of the concrete are significantly improved. BEUSHAUSEN *et al*. [21] enhanced the interfacial bonding strength of the weak zone by increasing the roughness of the interface. This increase in roughness resulted in a 220% improvement in the shear strength of the structure. In order to improve the interlayer bonding strength of 3D printed concrete, WANG *et al*. [22, 23] applied mortar containing different polymers to the interlayer, and experimental results show that adding 8% epoxy resin to the mortar will increase the flexural strength by 222-277%. HOSSEINI *et al*. [24] formed a new polymer consisting of black carbon and sulfur was used to glue the two layers together, and the testing results show that the modified mortar could increase the flexural strength by 100%. A large number of researchers have effectively improved the interlayer properties of 3D printed concrete structure through different methods [25, 26]. However, the coatings utilized by the aforementioned researchers to enhance the properties of the interlayer interface need to be procured separately, thereby increasing the workload of operators in experiments or engineering. In the preliminary work, the author discovered an easy method that involves using thioaluminate cement and water with a water-cement ratio of 0.5 to create a cement slurry. This cement slurry exhibits excellent fluidity and adhesion. By applying this slurry between the layers of 3D printed concrete, it effectively improves the adhesion between the layers of 3D printing mortar. Therefore, the author of this paper aims to enhance the interlayer bonding performance of 3D printed mortar by refining the composition of inorganic coatings.

In previous research work [27], it was found that the cement slurry coating (C-coating), prepared with sulphoaluminate cement and water at a water-cement ratio (w/c) of 0.5, has a significant enhancement effect on the performance of cement-based materials. Additionally, it can also achieve the effect of using local materials. And the performance of the coating is further improved by incorporating fly ash and expansion agent into sulfoaluminate cement (F-coating and E-coating). The above three inorganic coatings (C-coating, F-coating, E-coating) were finally used to improve the performance of the printing mortar. The study involved testing the mechanical properties of the specimens through flexural strength and compressive strength measurements. The bond strength was evaluated using bond strength and micro indentation technique. The hydration products were analyzed using X-ray diffraction (XRD), and the microstructure was observed using a scanning electron microscope (SEM).

## 2. MATERIALS AND METHODS

### 2.1. Raw materials and mix proportions

The calcium sulfoaluminate cement (CSA) 42.5 used in this study was provided by Dalian Onoda Cement Co. Ltd. Fly ash (FA) and expansion agent (EA) were obtained from Henan Hengyuan New Materials Co. Ltd. The main chemical compositions of these materials are presented in Table 1. The fine aggregate used was quartz sand with a size range of 0.1 mm to 0.8 mm.

In this study, three types of cement slurry mixed with various additives were chosen as interlayer reinforcement materials. In the previous research conducted by the author's research group, it was determined that the coating should be applied using a cement slurry with a w/c of 0.5 [27], and the material mixing ratios of the three types of coatings are presented in Table 2.

**Table 1:** Chemical composition of cementitious materials (%).

| Sample | $SiO_2$ | MgO | CaO | $Fe_2O_3$ | $SO_3$ | $Al_2O_3$ | $TiO_2$ |
|---|---|---|---|---|---|---|---|
| CSA | 6.13 | 1.24 | 42.54 | 1.53 | 10.79 | 35.17 | – |
| FA | 52.97 | 1.71 | 6.27 | 5.27 | 1.46 | 28.77 | 1.66 |
| EA | 1.03 | 1.81 | 52.56 | 0.66 | 28.33 | 13.61 | 0.02 |

**Table 2:** Mixing ratios of three coating materials (%).

| SAMPLE | CSA | FA | EA |
|---|---|---|---|
| C-coating | 100 | – | – |
| F-coating | 94 | 6 | – |
| E-coating | 94 | – | 6 |

### 2.2. Sample preparation

The 3D printing equipment (shown in Figure 1) in this study was provided by Dalian Xueqing Mingfeng numerical control technology Co. Ltd. The printer realizes multi-functional integrated 3D printing, which is composed of storage system, dry powder circulation system, printing system, computer numerical control device and machine tool body. The maximum size of the printing concrete specimen is 1.5 m × 1 m × 0.6 m.

In order to achieve rapid setting of cementitious materials in 3D printing, the process involves conveying dry powder materials into a feeding bin, which are then transferred to the circulation system by a spiral winch. The material is delivered to the printing system through a combination of stirring blade action and gravity. Water is pumped into the system, with the flow controlled by a meter. Within the printing system, the dry material is mixed with water. The cement mortar is then extruded by a rotating print head, and the 3D object is built up by moving the guide rail to complete the printing process.

The 3D concrete printer is utilized to print cement mortar by following a predetermined printing path. The printing parameters for this process are as follows: the spindle speed is set at 600 r/min, the travel speed is set at 1200 mm/min. The printing head has a circular section with a diameter of Φ18mm, and the printing thickness is 18.5mm. During the printing process, after each layer of printing is completed, coating (1 mm) is added by coating jetting equipment to the top surfaces of the last layer.

### 2.3. Testing and analysis techniques

The hardened mortar was cut into the specimens with 160 mm × 40 mm × 40 mm and 40 mm × 40 mm × 40 mm for mechanical properties test [28]. The cut specimens are shown in Figure 2. The mortar specimens were placed in the curing box (temperature 25°C, humidity 95%) to the specified age (7days, 28days), and the flexural strength and compressive strength tests were carried out according to "Test Method of Cement Mortar Strength" (GB/T 17671-1999).

The test method of interlayer bonding strength refers to "Test Method Ordinary of Mechanical Properties on Ordinary Concrete" (GB/T 50081-2002). The size of mortar specimens are 40 mm × 40 mm × 40 mm, and two steel tubes were placed at the interlayer junction of specimen (as shown in Figure 3). The average value of the test results of 6 specimens in each group was taken as the final test result.

After samples grinded and polished, the micron indentation test was carried out with the help of the micron mechanical test system (shown in Figure 4) which is independently developed by China Building Materials Academy Co. Ltd. The loading speed is 0.5 mm/min, the loading and unloading time is separately 30s, and the maximum load is fixed as 1.5 mN to obtain the hardness of the selected area. To ensure the accuracy

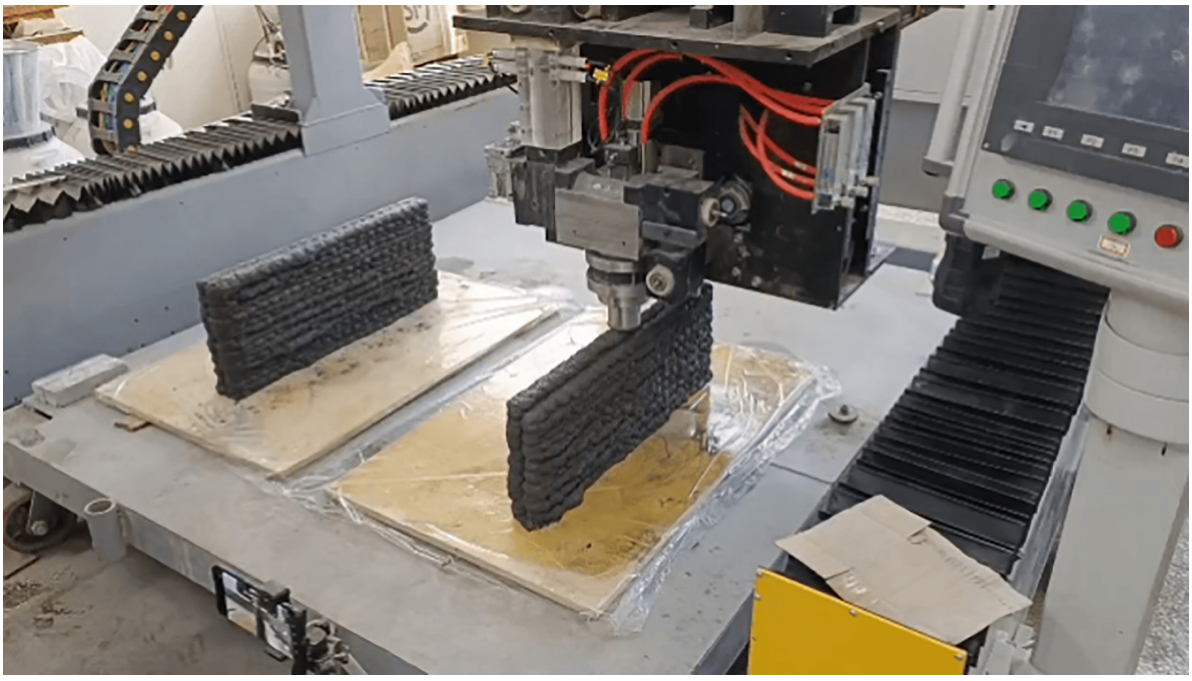

**Figure 1:** 3D printing equipment.

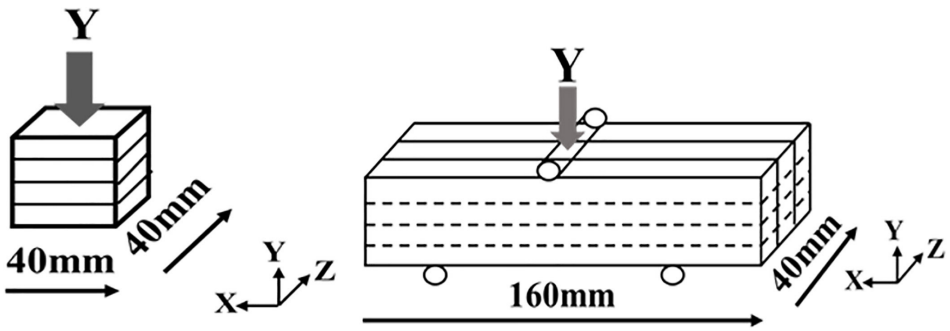


**Figure 2:** The cut specimens for mechanical properties test.

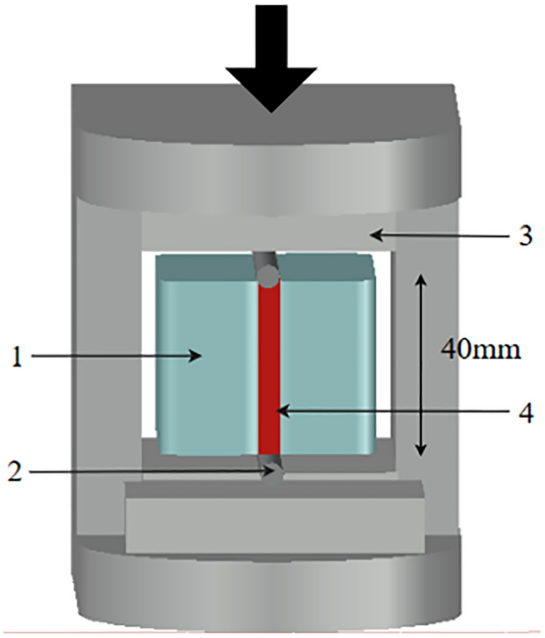


**Figure 3:** The Bond strength test (1. Mortar, 2. Steel tube, 3. Loading plate, 4. Coating).

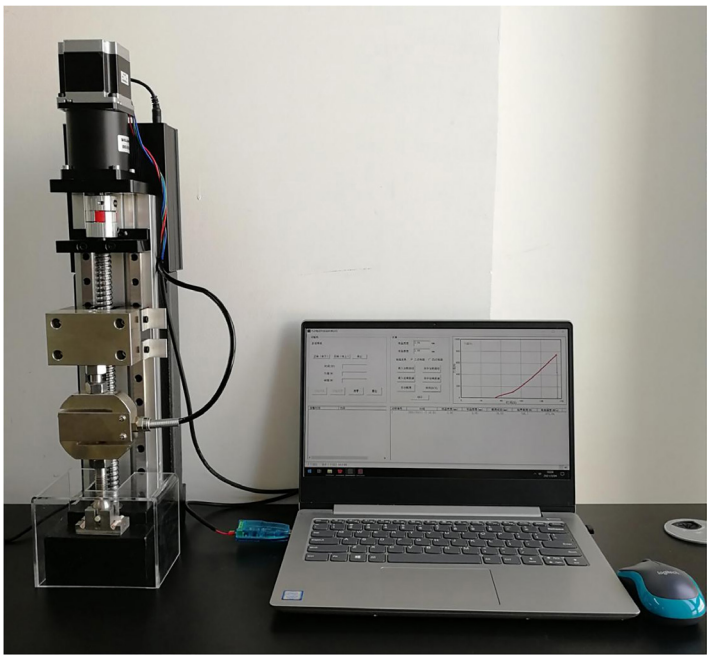

**Figure 4:** The micron mechanical test system.

of the data, the needle pressing step is controlled at 20 mm. The test from mortar to coating was carried out in a straight line to avoid pores and cracks. 7 points were hit in each set of tests, and each value was the average of the three actual measurements.

An Empyrean X-ray diffractometer was used for XRD with 60 kV tube voltage and 50 mA tube current. The measurable 2θ range was 15° to 50°, and the scan rate was 4°/min. A JSM-6360LV stereo scanner was used for observation and photographing. The acceleration voltage of the scanner was 20 kV, the resolution was 20 nm, the magnification was 500-30,000, the working voltage was 112 kV, the working current was 5mA, and the spraying thickness was 15–20 nm.

## 3. RESULTS AND DISCUSSIONS

### 3.1. The flexural strength

The test results of the flexural strength of the 3D printed mortar with/without three different inorganic coatings at the age of 7 days and 28 days are shown in the Figure 5. It can be seen that inorganic coatings could significantly enhance the flexural strength of printed mortar. Compared with the specimens without coating, the flexural strength of the specimens coated with C-coating, F-coating and E-coating increases by 24%, 42% and 37% at 7d, respectively. The flexural strength of specimens coated with C-coating, F-coating and E-coating increased by 24%, 35% and 27% at 28d compared with plain specimens. This indicates that the addition of all the three inorganic coatings could significantly improve the flexural strength of printed mortar, and the mortar with F-coating improves the most.

### 3.2. The compressive strength

Figure 6 shows the compressive strength test results of 3D printed mortar with/without three inorganic coatings at curing age 7 days and 28 days.

It could be seen that the variation of compressive strength is similar to that of flexural strength. Compared with that of the specimens without coating, when the curing age is 7 days, the compressive strength of the 3D printed mortar specimen is increased by 22% by C-coating, 30% by F-coating, and 26% by E-coating. When the curing age is 28 days, the compressive strength of the specimens coated with C-coating, F-coating and E-coating increases by 13%, 31% and 21%, respectively. The results of flexural strength test and compressive strength test show that among the three inorganic coatings, F-coating has the most obvious improvement effect on the mechanical properties of printed mortar, followed by E-coating, and finally C-coating.

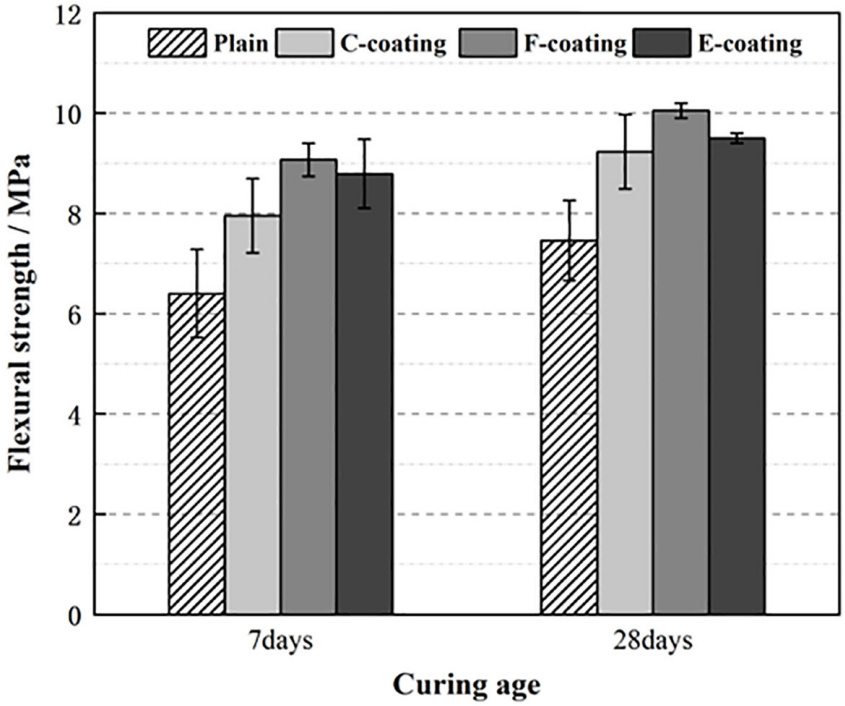


**Figure 5:** The flexural strength of the 3D printed mortar.

### 3.3. The bond strength

The test results of interlayer bond strength are shown in Figure 7. It can be seen from the test results that the three inorganic coatings could significantly improve the bond strength between cement mortar layers. Compared with the specimens without coating, the bond strength increases by 71% when F-coating was added, 42% when E-coating was added, and only 7% when C-coating was added. Through the analysis of the results of bond strength test, flexural strength test and compressive strength test, it can be found that the mortar composition of all specimens is the same, but the mechanical properties are very obvious differences, indicating that the addition of coating will significantly enhance the bond strength of the interlayer interface, thus affecting the mechanical properties of cement mortar. The different composition of coatings also affect the bond strength of coatings, and the mechanical properties of cement mortar specimens with different coatings are obviously different.

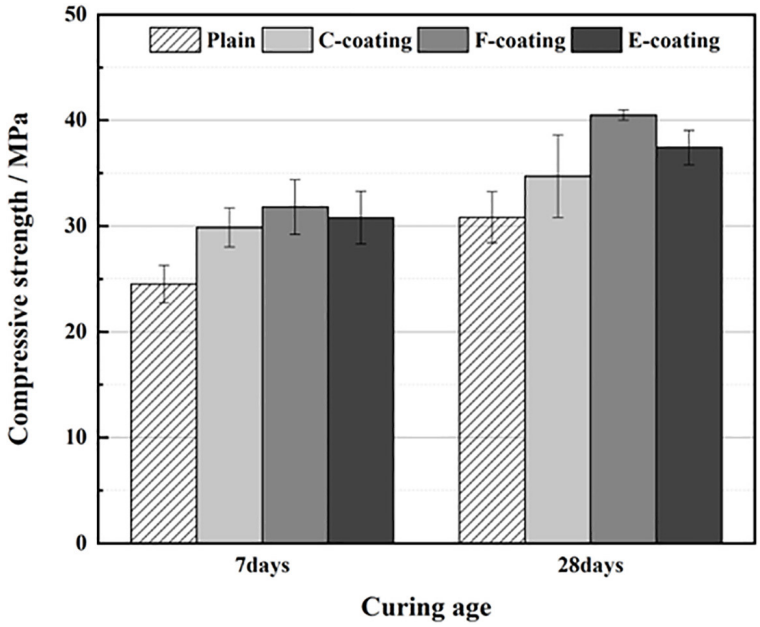


**Figure 6:** The compressive strength of the 3D printed mortar.

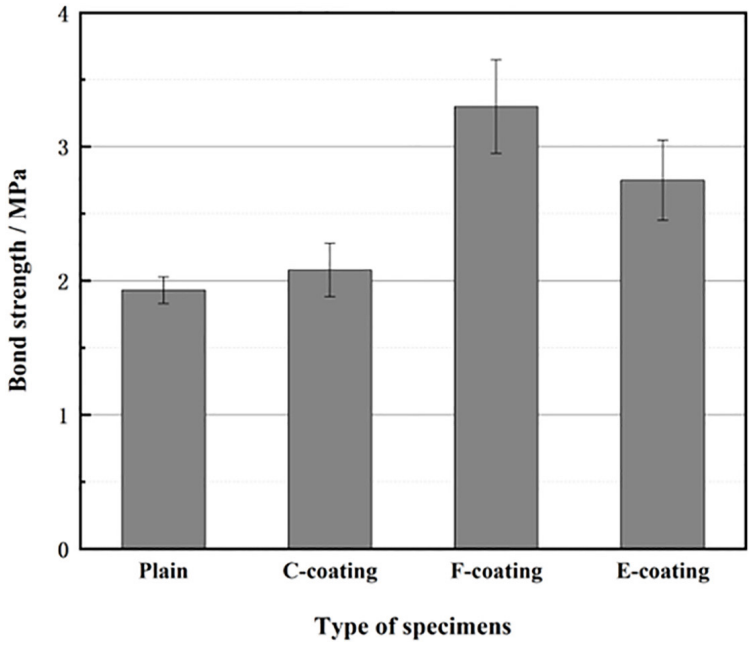


**Figure 7:** The bond strength of coatings.

### 3.4. The micron indentation

The micron indentation test results of mortar and coating are shown in the Figure 8. The hardness of mortar is about 100HV, the hardness of coating is 60-75 HV, and the interfacial transition zone (ITZ) between mortar and coating has the lowest hardness (61–69 HV). The maximum indentation displacement (MID) of mortar is about 100 μm, the MID of coating is 180-280 μm, and the MID of ITZ is 250–300 μm. The results show that the addition of three inorganic coatings increases the bonding strength between the mortar layers, but it is inevitable that a new weakness zone of bonding property will be formed between the coating and the mortar layer when coatings are added.

Among the three types of coatings, the hardness of F-coating is 72–74 HV, that of E-coating is 63–68 HV and that of C-coating is 62-65 HV, indicating that the hardness of F-coating is the highest among the three types of inorganic coatings. It is worth noting that the hardness of F-coating and mortar layer in ITZ area is significantly higher than the other two coatings, and the hardness of E-coating and C-coating in ITZ area is basically equal.

### 3.5. XRD

As the main raw material of the three types of inorganic coatings is CSA, the crystal types and the amount crystals of coatings of all specimens had no significant difference. The hydration products are still mainly Ettringite (AFt), Calcium hydroxide (CH) and Aluminum hydroxide ($AH_3$). Figure 9 shows the peaks of AFt, CH and $AH_3$ of XRD patterns. In order to accurately detect the crystal composition of coatings, the fracture surface of specimens of the bonding strength was selected, and about 1 mm of the thickness of the upper surface of the fracture surface was cut and ground into powder. In this study, the content of hydration products in different coatings is indirectly compared by comparing the peak value. The AFt crests at 15.5º–18.0º and 22.5º–23.5º (2θ), the CH crests at 18.4º–19.2º and 34.5º–23.5º (2θ), the $AH_3$ crests at 18.4º–19.2º and 34.5º–23.50º (2θ). It can be seen from Figure 9 that the peak of AFt (2θ = 15.8º) for E-coating was 5800, C-coating was 5000, the peak of AFt for F-coating was 5000.

The order of peak values of CH is basically the same as that of AFt. The CH crests value of E-coating is the highest, followed by C-coating and F-coating is the lowest. However, the order of peak values of $AH_3$ is different from the above two results, being C-coating>F-coating>E-coating.

### 3.6. SEM

In order to explore the influence of different coatings on the morphology of interlayer interface, C-coating, E-coating, and F-coating specimens were selected. Figure 10 shows the micromorphologies of the three types of inorganic coatings.

It can be seen from the electronic scanner photograph (Figure 10a) that there are a large number of pores and CH crystals inside the C-coating, there were a large number of unhydrated substances. What can be seen from Figure 10b is that there are a lot of C-S-H gels (amorphous colloidal form [12]) inside the F-coating, and these dense gels are evenly distributed at interlayer interface. In Figure 10c, a large number of CH and AFt exist in the pores of E-coating, and acicular AFt crystals and tabular CH crystals intersperse increase the adhesion of mortar. The two crystals filled part of the pores, but the filling ability is poorer than C-S-H gels.

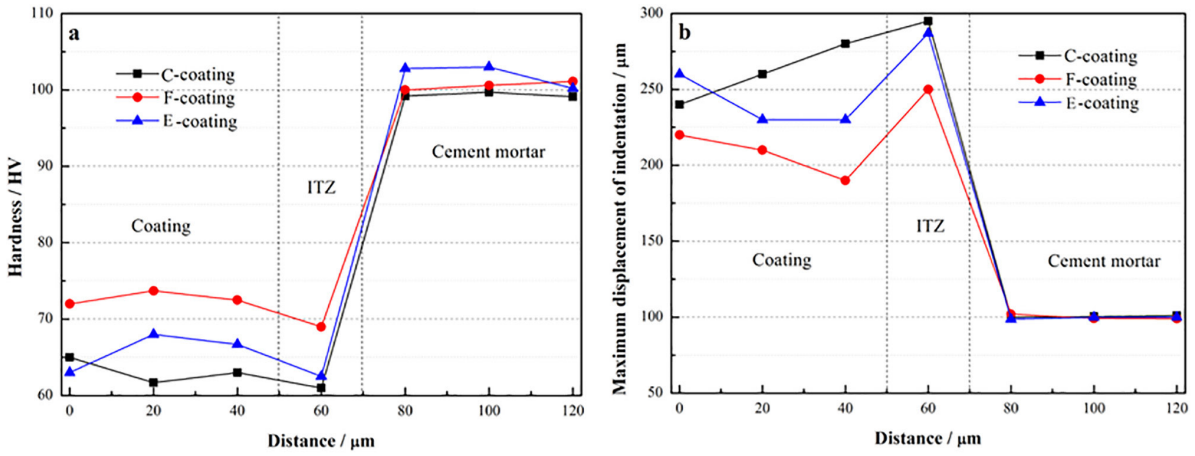


**Figure 8:** The micron indentation test of specimens: (a) Hardness of specimens; (b) MID of specimens.

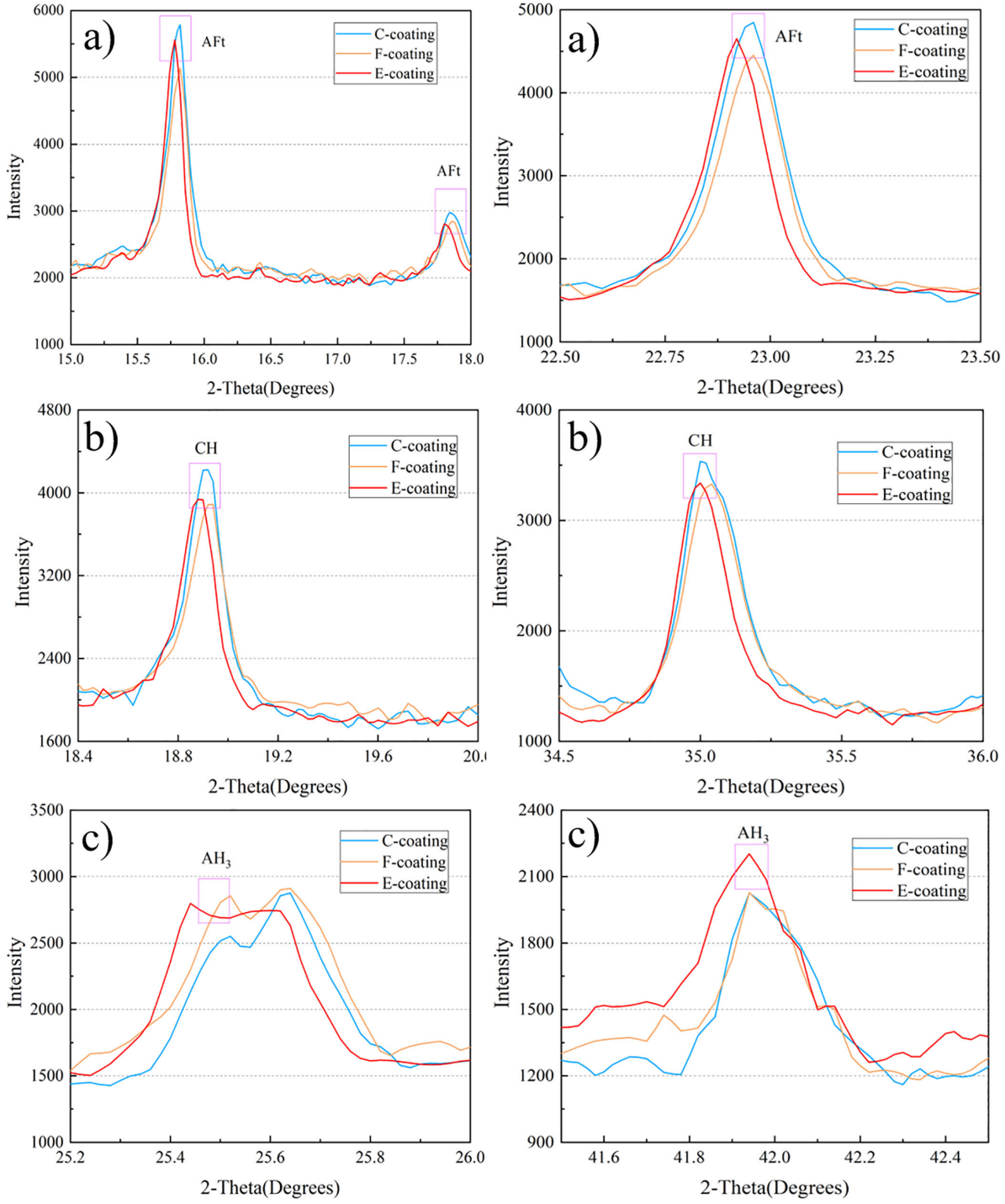


**Figure 9:** The XRD pattern of coatings: (a) the peak value of AFt; (b) the peak value of CH; (c) the peak value of $AH_3$.

### 3.7. The influence mechanism of coatings on cement mortar

The test results of XRD and SEM show that, compared with the other two coatings. When $C_4A_3\check{S}$ reacts with water alone at low water/solid ratios, it produces mono-sulfoaluminate ($C_4A_3\check{S}H_{12}$ or Ms12) and aluminium hydroxide ($AH_3$), show in equation (1). In environments with higher water content, the presence of ettringite ($C_6A\check{S}_3H_{32}$ or AFt) can also be observed. The hydration of $C_4A_3\check{S}$ with calcium sulfate ($C\check{S}$) results in the formation of AFt and $AH_3$, show in equation (2). When a certain amount of $C\check{S}$ and calcium hydroxide (CH) are present in the system, two specific hydration reactions occur, leading to the formation of mono-sulfoaluminate and ettringite as the final hydration products, show in equation (3) and equation (4) [29]. The AFt and CH generated in the E-coating can be inserted into the mortar matrix to act like fibers.

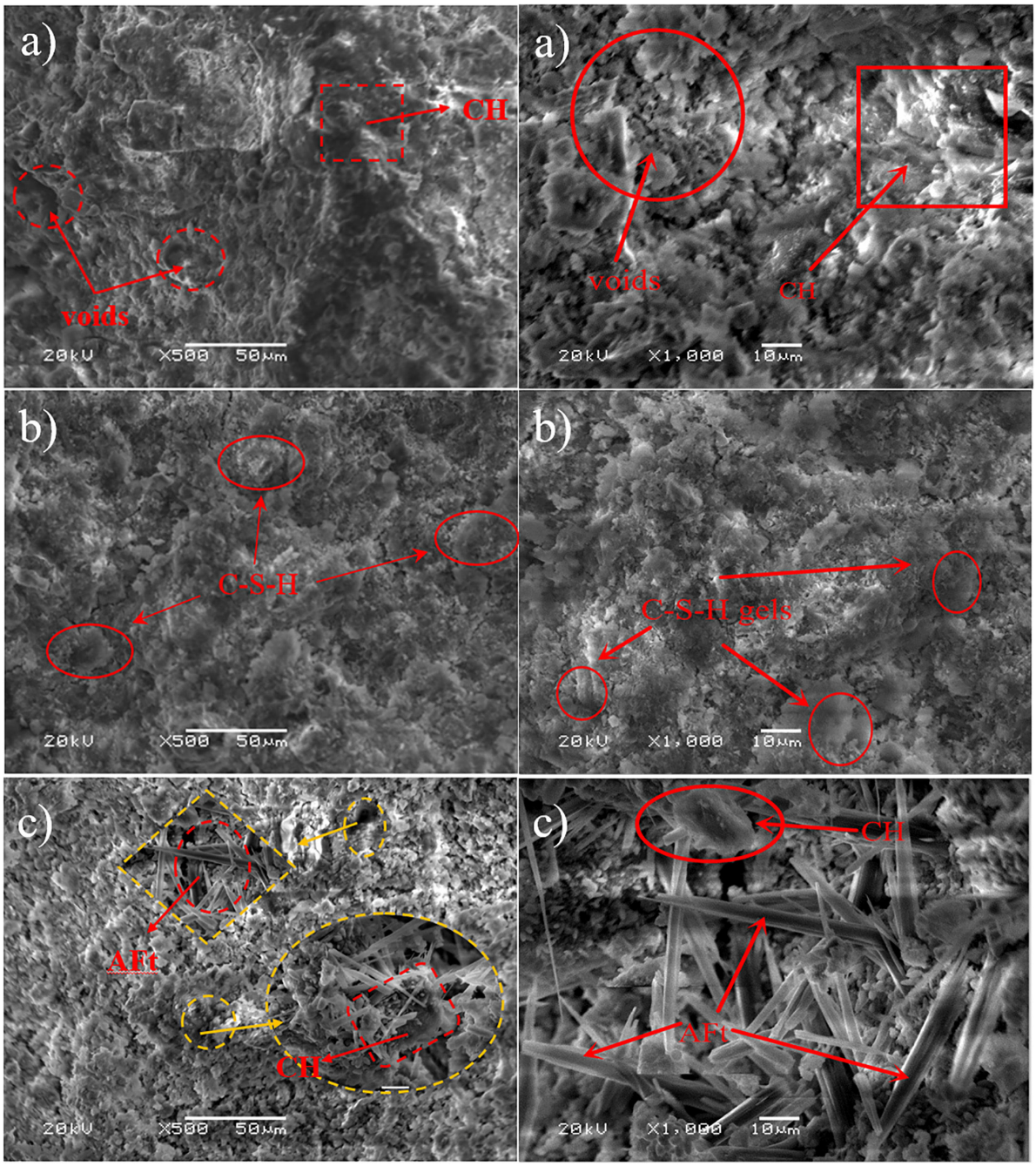


**Figure 10:** The microstructure of three types of coatings: (a) C-coating; (b) F-coating; (c) E-coating.

$$C_4A_3\check{S} + 18H \rightarrow C_4A_3\check{S}H_{12} + 2AH_3 \quad (1)$$

$$C_4A_3\check{S} + 2C\check{S}H_2 + 34H \rightarrow C_6A\check{S}_3H_{32} + 2AH_3 \quad (2)$$

$$C_4A_3\check{S} + 2C\check{S}H_2 + 6CH + 26H \rightarrow 3C_4A_3\check{S}H_{12} \quad (3)$$

$$C_4A_3\check{S} + 8C\check{S}H_2 + 6CH + 74H \rightarrow 3C_6A\check{S}_3H_{32} \quad (4)$$

The mechanical properties of F-coating is the best one among the three types inorganic coatings, which is also consistent with above conclusions on bond strengths. AFt and CH content in F-coating is lower, because the

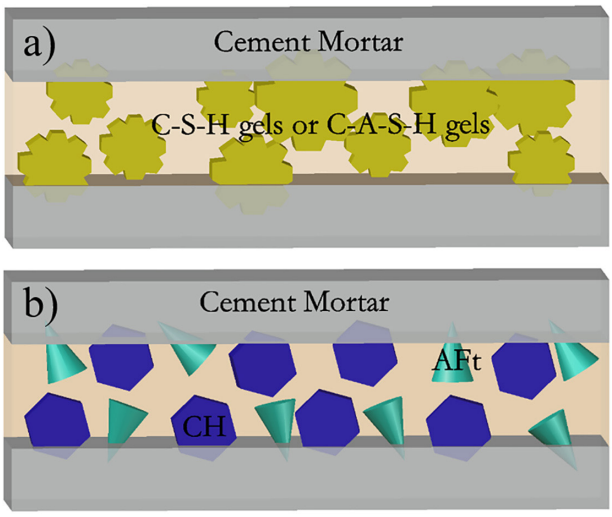


**Figure 11:** The hydration products in interlayer interface: (a) C-S-H gels or C-A-S-H gels of F-coating; (b) AFt and CH of E-coating.

main components of fly ash are $SiO_2$ and $Al_2O_3$, which will react with AFt and CH and will reduce the contents of AFt and CH. [30] C-S-H gels or C-A-S-H gels (Figure 11a) with higher compactness and better mechanical properties were generated while AFt and CH contents were reduced.

The content of AFt and CH in E-coating is higher than that of C-coating and F-coating. This is because E-coating contains a large amount of CaO (> 50%) [27], which will promote the formation of AFt and CH. The AFt and CH hydration products could increase the early mechanical properties (Figure 11b). Compared with C-S-H gels, these two hydration products show high brittleness and low compactness, so the strength of E-coating is lower than that of F-coating. Therefore, the enhancement effect of E-coating on the mechanical properties of 3D printed mortar is inferior to F-coating, but better than C-coating.

## 4. CONCLUSIONS

This study investigates the impact of three types of inorganic coatings applied to the interlayer zone of 3D printed mortar. Mechanical properties such as compressive strength and flexural strength were analyzed, while the bond strength of the interlayer zone was assessed through splitting and micron-indentation tests. The influence of coatings on hydration characteristics was explored using XRD, and the microstructure of the interlayer zone was examined with SEM. The findings and discussions lead to the following conclusions.

(1) Three types of inorganic coatings (C-coating, F-coating, and E-coating) were found to enhance the flexural strength (24%, 35%, 27%), compressive strength (13%, 31%, 21%), and bond strength (7%, 71%, 42%) of 3D printed mortar at 28 days. The results indicated that E-coating and F-coating had a significant positive impact on the mechanical and bonding properties of 3D printed mortar, while C-coating did not show effective improvement in these properties.

(2) E-coating is likely to increase the content of AFt and CH at the interlayer zone due to the high CaO content (> 50%) in the expansion agent, which promotes the formation of AFt and CH while decreasing the Al element content. On the other hand, F-coating is expected to reduce AFt and CH contents because fly ash, the main components of which are $SiO_2$ and $Al_2O_3$, lowers the Ca element content. Additionally, fly ash reacts with AFt and CH to form C-S-H gels or C-A-S-H gels.

(3) The results of micron indentation test and SEM test indicate that neither F-coating nor E-coating can significantly enhance the hardness of hydration products. However, their characteristics enable hydration products to function similarly to fibers, enhancing the connectivity between layers and increasing the density of the interlayer zone. Consequently, when F-coating and E-coating are added to interlayers of 3D printing mortar, there is a notable enhancement in the overall mechanical properties.

(4) The raw materials of the three coatings are all common materials in the laboratory. These raw materials can achieve rapid synthesis of coatings with reasonable mixing ratios. The authors determined through experiments the mix ratio parameters of two coatings that are both easily available and can effectively improve the interlayer bonding properties. This paper provides data for 3D printing interface transition zone improvement methods.

## 5. ACKNOWLEDGMENTS

The financial support from Key science and technology research and development projects of Dalian (No. 2023YF23WZ045), the Key Project of the National Natural Science Foundation of China (No. 52032011), and Key Laboratory Platform Open Project of Liaoning Province (No. DLSZD2023[009]).

## 6. BIBLIOGRAPHY

[1] BUSWELL, R.A., LEAL DE SILVA, W.R., JONES, S.Z., *et al*., "3D printing using concrete extrusion: a roadmap for research", *Cement and Concrete Research*, v. 112, pp. 37–49, Oct. 2018. doi: http://doi.org/10.1016/j.cemconres.2018.05.006.

[2] DE SCHUTTER, G., LESAGE, K., MECHTCHERINE, V., *et al*., "Vision of 3D printing with concrete — Technical, economic and environmental potentials", *Cement and Concrete Research*, v. 112, pp. 25–36, Oct. 2018. doi: http://doi.org/10.1016/j.cemconres.2018.06.001.

[3] MAZHOUD, B., PERROT, A., PICANDET, V., *et al*., "Underwater 3D printing of cement-based mortar", *Construction & Building Materials*, v. 214, pp. 458–467, Jul. 2019. doi: http://doi.org/10.1016/j.conbuildmat.2019.04.134.

[4] ALGHAMDI, H., NEITHALATH, N., "Synthesis and characterization of 3D-printable geopolymeric foams for thermally efficient building envelope materials", *Cement and Concrete Composites*, v. 104, pp. 103377, Nov. 2019. doi: http://doi.org/10.1016/j.cemconcomp.2019.103377.

[5] SUIKER, A.S.J., WOLFS, R.J.M., LUCAS, S.M., *et al*., "Elastic buckling and plastic collapse during 3D concrete printing", *Cement and Concrete Research*, v. 135, pp. 106016, Sep. 2020. doi: http://doi.org/10.1016/j.cemconres.2020.106016.

[6] JI, G., DING, T., XIAO, J., *et al*., "A 3D printed ready-mixed concrete power distribution substation: materials and construction technology", *Materials (Basel)*, v. 12, n. 9, pp. 1540, May. 2019. doi: http://doi.org/10.3390/ma12091540. PubMed PMID: 31083405.

[7] SILVA, L.F., FILLA, G.D.T., AMORIM, E.M.R., *et al*., "Usage potential of fly ash an metakaolin in cementitious materials for 3D printing", *Matéria (Rio de Janeiro)*, v. 27, n. 2, pp. e13196, Feb. 2022. doi: http://doi.org/10.1590/s1517-707620220002.1396.

[8] LIU, C., CHEN, Y., ZHANG, Z., *et al*., "Study of the influence of sand on rheological properties, bubble features and buildability of fresh foamed concrete for 3D printing", *Construction & Building Materials*, v. 356, pp. 129292, Nov. 2022. doi: http://doi.org/10.1016/j.conbuildmat.2022.129292.

[9] CHE, Y., YANG, H., "Hydration products, pore structure, and compressive strength of extrusion-based 3D printed cement pastes containing nano calcium carbonate", *Case Studies in Construction Materials*, v. 17, pp. e01590, Dec. 2022. doi: http://doi.org/10.1016/j.cscm.2022.e01590.

[10] HAN, Y., YANG, Z., DING, T., *et al*., "Environmental and economic assessment on 3D printed buildings with recycled concrete", *Journal of Cleaner Production*, v. 278, pp. 123884, Jan. 2021. doi: http://doi.org/10.1016/j.jclepro.2020.123884.

[11] YANG, R., ZENG, Q., PENG, Y., *et al*., "Anomalous matrix and interlayer pore structure of 3D-printed fiber-reinforced cementitious composites", *Cement and Concrete Research*, v. 157, pp. 106829, Jul. 2022. doi: http://doi.org/10.1016/j.cemconres.2022.106829.

[12] LIU, C., CHEN, Y., XIONG, Y., *et al*., "Influence of HPMC and SF on buildability of 3D printing foam concrete: from water state and flocculation point of view", *Composites. Part B, Engineering*, v. 242, pp. 110075, Aug. 2022. doi: http://doi.org/10.1016/j.compositesb.2022.110075.

[13] NAIR, S.A.O., TRIPATHI, A., NEITHALATH, N., "Examining layer height effects on the flexural and fracture response of plain and fiber-reinforced 3D-printed beams", *Cement and Concrete Composites*, v. 124, pp. 104254, Nov. 2021. doi: http://doi.org/10.1016/j.cemconcomp.2021.104254.

[14] RAHUL, A.V., SANTHANAM, M., MEENA, H., *et al*., "Mechanical characterization of 3D printable concrete", *Construction & Building Materials*, v. 227, pp. 116710, Dec. 2019. doi: http://doi.org/10.1016/j.conbuildmat.2019.116710.

[15] NAPOLITANO, R., FORNI, D., MENNA, C., *et al*., "Dynamic characterization of the layer-interface properties of 3D-printed concrete elements", *Case Studies in Construction Materials*, v. 15, pp. e00780, Dec. 2021. doi: http://doi.org/10.1016/j.cscm.2021.e00780.

[16] TALEB, M., BULTEEL, D., BETRANCOURT, D., *et al*., "Interfacial weakness criterion by indentation in 3D printed concrete", *3D Printing and Additive Manufacturing*, v. 10, n. 2, pp. 318–329, Apr. 2023. doi: https://doi.org/10.1089/3dp.2021.0128.

[17] ZHANG, J., WANG, J., DONG, S., *et al*., "A review of the current progress and application of 3D printed concrete", *Composites. Part A, Applied Science and Manufacturing*, v. 125, pp. 105533, Oct. 2019. doi: http://doi.org/10.1016/j.compositesa.2019.105533.

[18] ZHANG, C., HOU, Z., CHEN, C., *et al*., "Design of 3D printable concrete based on the relationship between flowability of cement paste and optimum aggregate content", *Cement and Concrete Composites*, v. 104, pp. 103406, Nov. 2019. doi: http://doi.org/10.1016/j.cemconcomp.2019.103406.

[19] PAN, T., JIANG, Y., HE, H., *et al*., "Effect of structural build-up on interlayer bond strength of 3D printed cement mortars", *Materials (Basel)*, v. 14, n. 2, pp. 236, Jan. 2021. doi: http://doi.org/10.3390/ma14020236. PubMed PMID: 33418852.

[20] LI, Z., WANG, L., MA, G., "Method for the enhancement of buildability and bending resistance of 3d printable tailing mortar", *International Journal of Concrete Structures and Materials*, v. 12, n. 1, pp. 37, Dec. 2018. doi: http://doi.org/10.1186/s40069-018-0269-0.

[21] BEUSHAUSEN, H., ALEXANDER, M.G., "Bond strength development between concretes of different ages", *Magazine of Concrete Research*, v. 60, n. 1, pp. 65–74, Feb. 2008. doi: http://doi.org/10.1680/macr.2007.00108.

[22] WANG, L., MA, G., LIU, T., *et al*., "Interlayer reinforcement of 3D printed concrete by the in-process deposition of U-nails", *Cement and Concrete Research*, v. 148, pp. 106535, Oct. 2021. doi: http://doi.org/10.1016/j.cemconres.2021.106535.

[23] WANG, L., TIAN, Z., MA, G., *et al*., "Interlayer bonding improvement of 3D printed concrete with polymer modified mortar: experiments and molecular dynamics studies", *Cement and Concrete Composites*, v. 110, pp. 103571, Jul. 2020. doi: http://doi.org/10.1016/j.cemconcomp.2020.103571.

[24] HOSSEINI, E., ZAKERTABRIZI, M., KORAYEM, A.H., *et al*., "A novel method to enhance the interlayer bonding of 3D printing concrete: an experimental and computational investigation", *Cement and Concrete Composites*, v. 99, pp. 112–119, May. 2019. doi: http://doi.org/10.1016/j.cemconcomp.2019.03.008.

[25] YANG, R., ZHU, Y., LAN, Y., *et al*., "Differences in micro grain/fiber distributions between matrix and interlayer of cementitious filaments affected by extrusion molding", *Additive Manufacturing*, v. 60, pp. 103236, Dec. 2022. doi: http://doi.org/10.1016/j.addma.2022.103236.

[26] JIA, Z., HAN, Y., ZHANG, Y., *et al*., "Quantitative characterization and elastic properties of interfacial transition zone around coarse aggregate in concrete", *Journal of Wuhan University of Technology-Mater. Sci. Ed.*, v. 32, n. 4, pp. 838–844, Aug. 2017. doi: https://doi.org/10.1007/s11595-017-1677-8.

[27] PEI, Q., XIANG, Y., HU, S., *et al*., "Design analysis and test verification of double-layer gradient coating reinforced concrete flexural strength", *Journal of Nanomaterials*, v. 2022, pp. 6814947, Jun. 2022. doi: http://doi.org/10.1155/2022/6814947.

[28] KHALIL, N., AOUAD, G., EL CHEIKH, K., *et al*., "Use of calcium sulfoaluminate cements for setting control of 3D-printing mortars", *Construction & Building Materials*, v. 157, pp. 382–391, Dec. 2017. doi: http://doi.org/10.1016/j.conbuildmat.2017.09.109.

[29] CHANG, J., YU, X., SHANG, X., *et al*., "A reaction range for hydration of calcium sulfoaluminate with calcium sulfate and calcium hydroxide: theory and experimental validation", *Advances in Cement Research*, v. 28, n. 10, pp. 664-674, Nov. 2016. doi: http://doi.org/10.1680/jadcr.16.00045.

[30] GARCÍA-MATÉ, M., DE LA TORRE, A.G., LEÓN-REINA, L., *et al*., "Hydration studies of calcium sulfoaluminate cements blended with fly ash", *Cement and Concrete Research*, v. 54, pp. 12–20, Dec. 2013. doi: http://doi.org/10.1016/j.cemconres.2013.07.010.